Egypt. J. Chem. **Vol. 68**, No. 12 pp. 213 - 224 (2025)

Egyptian Journal of Chemistry

http://ejchem.journals.ekb.eg/

ZnO doped Fe_3O_4/Activated carbon Composite for High Efficient Photocatalytic Degradation of Congo red Dye

Fahma Riyanti[1], Erida Novrilia[1], Fatma[1], Desnelli[1], Widia Purwaningrum[1], Poedji Loekitowati Hariani[1]*

[1]*Department of Chemistry, Faculty of Mathematics and Natural Sciences, Universitas Sriwijaya, Ogan Ilir 30662, Indonesia*

Abstract

The widespread presence of dyes in water necessitates study to mitigate these hazardous substances. The current investigation synthesized Fe_3O_4/activated carbon (AC) doped with ZnO to create the Fe_3O_4/AC@ZnO composite, utilized for the photocatalytic degradation of Congo red dye. Activated carbon was produced from bamboo utilizing KOH as an activator. The synthesized Fe_3O_4/AC@ZnO composite was characterized utilizing various instruments, including X-ray Diffraction (XRD), Fourier Transform Infrared Spectroscopy (FTIR), Scanning Electron Microscopy with Electron Dispersive X-ray Spectroscopy (SEM-EDS), Vibrating Sample Magnetometry (VSM), BET surface area analysis. The absorbance of Congo red dye was assessed UV-Vis Diffuse Reflectance Spectroscopy (UV-Vis DRS). Fe_3O_4/AC@ZnO composite exhibits magnetic properties with a magnetic moment of 59.37 emu/g, a bandgap of 2.16 eV, and a surface area of 131.56 m^2/g. Fe_3O_4/AC@ZnO has tremendous performance as catalyst under visible light, achieving a 99.20% reduction of Congo red dye at pH 4, a dosage of 0.3 g/L, a dye concentration of 20 mg/L, and an irradiation time of 80 min. Furthermore, the catalyst exhibits significant stability, with an efficiency of 92% after five repetitions. The superoxide anion ($\bullet O_2^-$) plays a fundamental function in degradation. The pseudo-first-order model effectively describe the kinetic behavior of the photocatalytic degradation of Congo red dye.

Keywords: Fe_3O_4/AC@ZnO composite; magnetism; photocatalytic degradation; Congo red; recycle

1.Introduction

Population increase, industrial advancement, and water contamination are significant issues currently[1]. Industries include textiles, paper, cosmetics, soap, and printing, generating liquid waste containing dyes [2]. Dyes pose a risk to aquatic ecosystems when discharged into water bodies untreated [3]. Approximately 20% of the colors utilized are discharged as waste [4,5]. Azo dyes are used in approximately 60%–70% of industrial dyes worldwide. The coloring agents that classified as Azo dyes containing azo groups (-N=N-) and benzidine groups. These dyes exhibit water solubility, in addition to carcinogenic and highly toxic, and indicate resistance to degradation due to their complex aromatic structure [6,7].

An excessive amount of dye compounds, elevated chemical oxygen demand (COD), and biological oxygen demand (BOD) also suspended particles are common in wastewater [8,9]. Congo red dye is frequently utilized in industrial applications. This dye is highly poisonous and possesses carcinogenic qualities that induce DNA alterations and promote the formation of cancer cells; it also leads to skin irritation and anaphylactic shock [10-12]. Congo red exhibits excellent solubility in water and is resistant to biological decomposition [13,14]. Currently, numerous methods have been utilized in mitigating Congo red dye from aqueous solutions, including adsorption [15], electrocoagulation-electro-oxidation [16], and membrane filtering [17]. Typically, these approaches exhibit drawbacks like prolonged treatment duration, sludge generation, elevated treatment expenses, and the production of secondary pollutants [18,19]. Consequently, the advancement of rapid, efficient, and cost-effective technology is necessary to address the constraints of these treatment approaches [20]. Photocatalytic degradation is regarded as an effective technique for eliminating dye-contaminated wastewater, with benefits such as high efficacy, simplicity, and eco-friendliness. Photocatalysts can entirely degrade dyes into non-harmful substances such as CO_2 and water when exposed to UV or visible light irradiation [21,22].

ZnO is an n-type semiconductor noted for its superior photocatalytic properties, nontoxic nature, affordability, electrical conductivity, and chemically stable properties[23,24]. However, the application of ZnO as a catalyst is constrained by the mechanism of recombination. ZnO possesses an energy band gap of around 3.37 eV, and the substantial energy necessary to excite electrons results in a propensity for rapid recombination of electrons and holes post-excitation. This renders ZnO significantly deficient in attaining elevated photocatalytic efficiency [25,26].Recombination and enhanced absorption within the range visible light can be mitigated through doping with various materials, including graphene-ZnO [27], CuO/ZnO [28], ZnO/Fe_2O_3 [29], ZnO-Doped Fe_3O_4/rGO [30], and ZnO-chitosan [31]. Activated charcoal (AC) modifies the properties of photocatalysts due to its high porosity, superior electron transport capability, and its capacity to prevent the agglomeration of

*Corresponding author e-mail: puji_lukitowati@mipa.unsri.ac.id; (Poedji LoekitowatiHariani)
Received date 23 February 2025; Revised date 01 April 2025; Accepted date22 April 2025
DOI: 10.21608/ejchem.2025.362947.11349

ZnO [32,33]. Doping activated carbon with ZnO (25:75) exhibits effective performance under UV radiation in the breakdown of methyl orange dye [34]. However, activated carbon possesses a bandgap energy between 3.0 and 3.6 eV, which restricts its efficacy in the ultraviolet domain.

This study developed activated carbon doped with Fe_3O_4 and ZnO. Fe_3O_4 is an n-type semiconductor characterized by a minimal bandgap energy of less than 2 eV [22]. Fe_3O_4 exhibits robust ferromagnetic characteristics, significantly enhancing the efficiency and environmental sustainability of the catalyst recovery process through magnetic separation. This study utilized activated carbon derived from bamboo, subsequently employing the Fe_3O_4/AC@ZnO composite for the degradation of Congo red dye under varying pH levels, composite dosages, and dye concentrations.

2. Materials and Methods

2.1 Activated carbon preparation

Bamboo stems were segmented into 1-2 cm lengths. The stems were subsequently rinsed using distilled water and sun-dried for 5 h. The stems were thereafter pounded to a size of ±1 mm. Bamboo underwent carbonization at a temperature of 300°C for an hour in a furnace. The carbon was pulverized and sifted to approximately 200 mesh. The carbon obtained was immersed in 1 M KOH at a ratio of 4:1 (40 mL KOH to 10 g carbon) for 24 h. Additionally, it was subjected to drying in an oven for 2 h at 105 °C. After that, the carbon was rinsed with 0.1 M HCl solution and distilled water until achieving a neutral pH. Activated carbon underwent carbonization at a temperature of 700°C for 5 h within nitrogen gas atmosphere. Finally, the activated carbon was dehydrated using an oven at 105°C for 3 h [35].

2.2.Synthesis of Fe_3O_4/AC

The synthesis was conducted via the coprecipitation technique. A total of 1.791 g of $FeCl_2{\cdot}4H_2O$ and 4.869 g of $FeCl_3{\cdot}6H_2O$ were solubilized in 50 mL of distilled water. The mixture was agitated at 200 rpm for 20 min employing a magnetic stirrer. Subsequently, 4 g of activated carbon was introduced with continuous agitation for 30 min while nitrogen gas was being circulated. A 2 M NaOH solution was added to the mixture incrementally and agitated for 30 min at 60°C until the pH reached around 10. The resultant magnetic composite was isolated with an external magnet and repetitively rinsed until achieving a neutral pH with distilled water. Fe_3O_4/activated carbon was underwent drying in an oven at 80°C for a duration of 2 h.

2.3.Synthesis of Fe_3O_4/AC@ZnO

2 g of Fe_3O_4/AC composite and 1.768 g of $ZnCl_2$ were added to 100 mL of distilled water. The mixture homogenized with a magnetic stirrer at 500 rpm at 80°C for four h. The pH of was altered by incrementally adding a 2 M NaOH solution. After that, the result was placed in a hydrothermal reactor for 12 h at150°C [3].

2.4. Characterization of materials

The phase structure and type were ascertained via X-Ray Diffraction (XRD) using a Rigaku Miniflex, while the optical properties of the material were evaluated through UV-VIS Diffuse Reflectance Spectroscopy (UV-VIS DRS) with a Pharmaspec UV-1700. Morphology and elements that constitute the materials were analyzed using Scanning Electron Microscopy coupled with Energy Dispersive Spectroscopy (SEM-EDS JSM 6510 LA). The measurement of surface area and pore size were performed using BET surface area analysis (Quantachrome Nova 4200e). The evaluation of magnetic qualities was evaluated using a Vibrating Sample Magnetometer (VSM Oxford 1.2 H). The Fourier Transform Infrared Spectroscopy (Perkin Elmer FTIR-1650) utilizing KBr pellets were employed to ascertain functional groups that possessed by the composite within the wavenumber range of 400–4000 cm^{-1}.

2.5. Photocatalytic activity

The photocatalytic degradation of Congo red dye was assessed with variations in the following variables: pH (4-10), catalyst dosege (0.1-0.4 g/L), and initial concentrations of dye (20-80 mg/L). The irradiation was performed using A 125-watt mercury lamp that positioned 15 cm from the Congo red dye solution within a reactor. Prior to irradiation, the Congo red dye solution, which had been combined with the composite, was positioned in a reactor in dark condition while being agitated to attain adsorption equilibrium during a duration of 40 min. Irradiation was conducted throughout a duration of 0 to 100 min, with intervals of 20 min. During procedure, thedegradation of the dye was assessed using a UV-Vis spectrophotometer (Model Orion Aquamate 8000).

3. Results and Discussion

3.1. XRD analysis

The XRD results of activated carbon, Fe_3O_4/AC, and Fe_3O_4/AC@ZnO are illustrated in Figure 1. Bamboo-derived activated carbon has a distinct broad peak associated with its amorphous structure at 2θ ~22.4° and ~43.6°. This peak corresponds to a crystal plane as described by the Miller indices (hkl) of (002) and (100) that are related to the turbostratic amorphous structure of the activated carbon indicating a low-level graphitic alignment of the crystalline carbonaceous structure. The identification of Fe_3O_4 in Fe_3O_4/activated carbon occurs at 2θ = 30.4◦, 35.7◦, 43.6◦, 53.7◦, 57.5◦, 62.9◦, and 74.2◦, corresponding to the indices (220), (311), (400), (422), (551), (440), and (553), respectively. The peak intensity is affected by the quantity of Fe_3O_4 in the composite [36]. The Fe_3O_4/AC@ZnO peak is primarily characterized by the peaks of Fe_3O_4 and ZnO. The ZnO peak is observed at 2θ = 31.80°, 34.44°, 36.28°, 47.59°, 56.65°, 62.92°, 68.49°, 69.55°, and 77.61°,

with the corresponding Miller index values of (100), (002), (101), (102), (110), (103), (112), (201), and (202). Certain peaks coincide between Fe_3O_4 and ZnO.

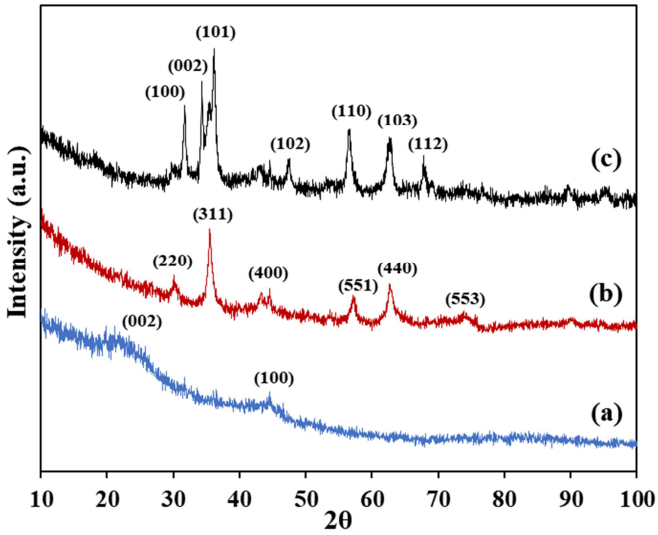

Figure 1: XRD spectra of (a) activated carbon, (b) Fe_3O_4/AC and (c) Fe_3O_4/AC@ZnO composite.

3.2. SEM -EDX analysis

Figure 2 depicts the surface morphology of activated carbon, Fe_3O_4/AC, and Fe_3O_4/AC@ZnO. Activated carbon possesses pores of unevenly distributed diameters. The incorporation of Fe_3O_4 leads to the clogging of some pores, akin to the integration of ZnO. Fe_3O_4 and ZnO can alter the surface morphology of activated carbon, increasing its roughness and enhancing the number of active sites for contact with pollutants. Rougher and coarser surfaces typically exhibit larger surface areas. The EDX statistics (Table 1) indicate that the presence of C, Fe, O, and Zn elements suggests successful synthesis.

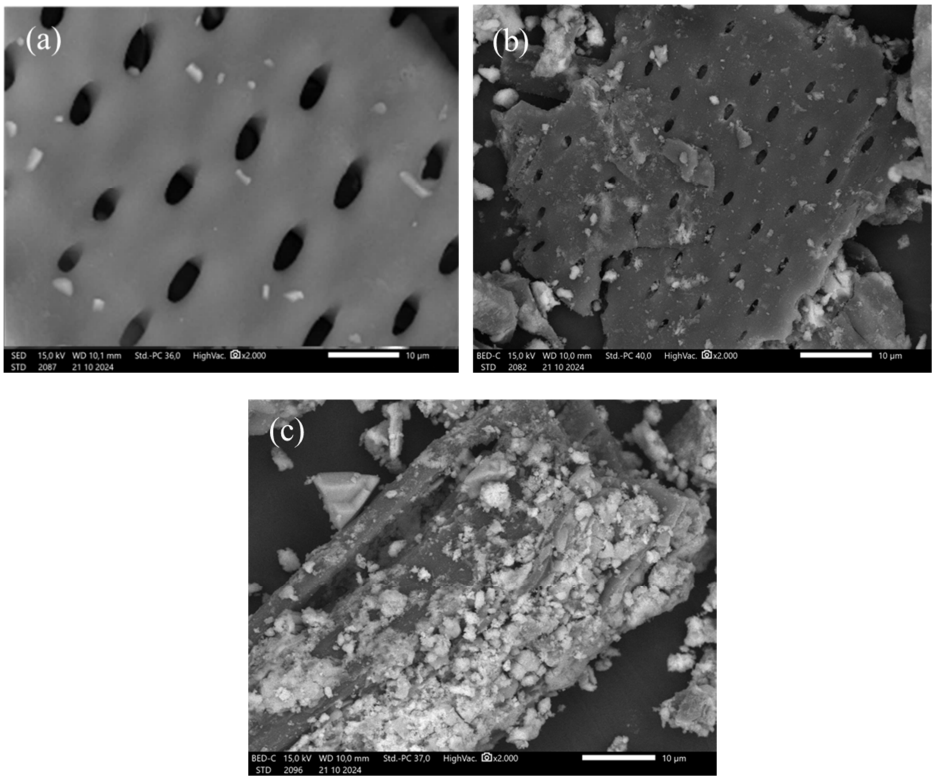

Figure 2: SEM image of (a) activated carbon, (b) Fe3O4/AC and (c) Fe3O4/AC@ZnO composite.

Table 1: Composition of the elements from the EDX analysis results

Materials	Elements (%)			
	C	O	Fe	Zn
Activated carbon	96.82	2.96	-	-
Fe_3O_4/AC	56.17	14.73	29.10	-
Fe_3O_4/AC@ZnO	42.45	22.87	24.23	9.45

3.3. BET surface area

Table 2 indicates that the inclusion of Fe_3O_4 and ZnO particles enhances the active surface area of activated carbon. The findings of Foroutan et al. [37] demonsrating the alteration of activated carbon derived from oak wood using Fe_3O_4 and ZnO enhanced the surface area. Similarly, this study found that activated carbon derived from bamboo had a surface area of 93.24 m²/g, which grew to 101.20 m²/g upon the incorporation of Fe_3O_4 and further to 131.56 m²/g following modification with both Fe_3O_4 and ZnO. Fe_3O_4 can physically interact with activated carbon, leading to alterations in its microstructure. Fe_3O_4 can occupy or create new pores in activated carbon, hence increasing the surface area. Moreover, diminutive Fe_3O_4 particles enhance the surface area relative to volume, consequently augmenting the effective surface area of the composite material. Activated carbon, Fe_3O_4/AC, and Fe_3O_4/AC@ZnO are categorized as mesoporous materials due to their typical pore diameter ranging from 2 to 50 nm [38].

Table 2: Surface area parameters

Materials	S_{BET} (m^2/g)	Pore Volume (cm^3/g)	Pore Diameter (nm)
Activated carbon	93.24	0.76	3.23
Fe_3O_4/AC	101.20	0.92	2.46
Fe_3O_4/AC@ZnO	131.56	1.15	2.44

3.4. UV-Vis DRS analysis

The optical characteristics of Fe_3O_4/AC and Fe_3O_4/AC@ZnO were analyzed via the UV–vis absorption spectrum, with findings illustrated in Figure 3. The optical properties of activated carbon were not assessed owing to its conductive characteristics. The absorption peak of Fe_3O_4/AC is at 396 nm, while Fe_3O_4/AC@ZnO is at a smaller wave number of 352 nm. ZnO typically exhibits a peak wavelength in the ultraviolet area. Aliah et al. [30] demonstrated that the absorption peak of ZnO was enhanced following its combination with Fe_3O_4 and rGO. In line with the bandgap value, Fe_3O_4/AC and Fe_3O_4/AC@ZnO each have a band gap value of 1.88 eV and 2.16 eV. A small bandgap value facilitates catalytic activity in the visible spectrum. An increased content of Fe_3O_4 in the composite correlates with a reduced bandgap value similar to other research where the ratio of Fe_3O_4:TiO_2 = 3:1 approaches the Fe_3O_4 bandgap value [39].

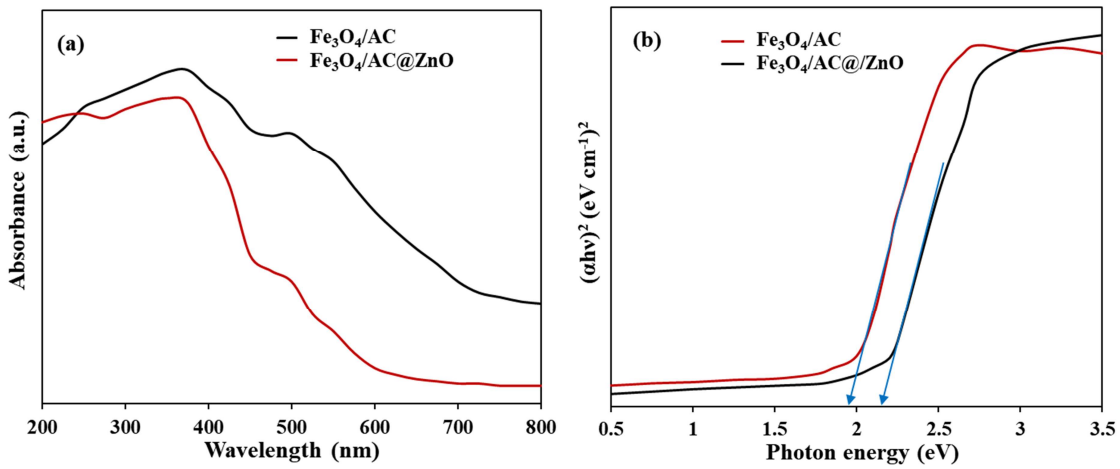

Figure 3: (a) UV–vis absorption and (b) Tauc plot of the Kubelka-Munk function of Fe_3O_4/AC and Fe_3O_4/AC@ZnO composite.

3.5. Magnetic moment analysis

The interaction between Fe_3O_4 and activated carbon may induce a dilution effect and alterations in the structure and size of Fe_3O_4 particles, leading to a reduced magnetic value of Fe_3O_4/AC compared to pure Fe_3O_4. Figure 4 indicates that Fe_3O_4/AC possesses a greater band gap than Fe_3O_4/AC@ZnO composite, measuring 74.43 emu/g and 59.37 emu/g, respectively. ZnO is a semiconductor characterized by a substantial band gap. The interaction between ZnO and Fe_3O_4 can influence the electronic structure or the local magnetic field surrounding the Fe_3O_4 particles, hence diminishing the capacity of

Fe_3O_4 to exhibit optimal magnetic characteristics. The magnetic characteristics of Fe_3O_4/AC@ZnO will allow a more efficient separation after degradation by using magnetic attraction instead of filtration.

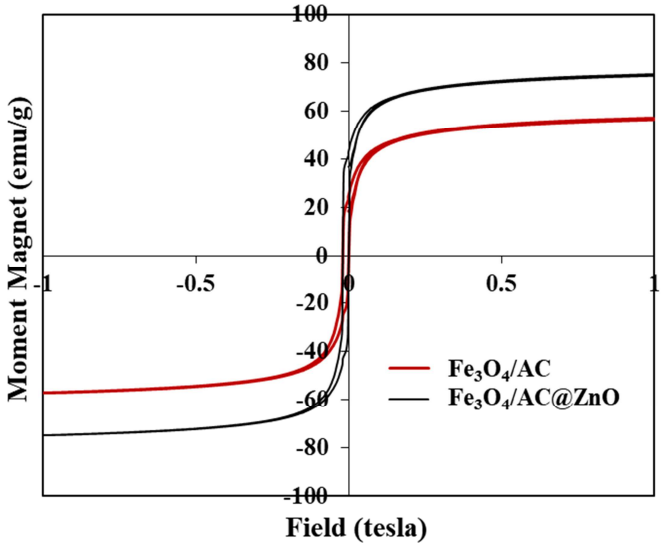

Figure 4: Hysteresis loops of Fe_3O_4/AC and Fe_3O_4/AC@ZnO composite.

3.5. FTIR analysis

Figure 5 diplays the FTIR result of activated carbon, Fe_3O_4/AC, and Fe_3O_4/AC@ZnO composite. Peaks at wave numbers approximately 3400 cm^{-1} and 1600 cm^{-1} in all spectra signify the stretching and vibration of adsorbed water molecules or the presence of O–H from phenolic compounds [40]. The absorption peak at 1500–1600 cm^{-1} in activated carbon results from the vibration of the C=C bond in alkenes within the aromatic ring [41]. The peak is not distinctly observable in the Fe_3O_4/AC and Fe_3O_4/AC@ZnO composites. The wave numbers 1000–1300 cm^{-1} signify the presence of C–O stretching vibrations, while the absorption peak at 2900-3000 cm^{-1} relates to C–H stretching vibrations. Absorption in the range of 400–600 cm^{-1} is indicative of metal oxides. This peak is not discernible in activated carbon. The Fe-O peak is distinctly observed at a wavenumber of 557 cm^{-1}. The Zn-O presence is shown by absorptions at 840 cm^{-1} and 420 cm^{-1} in the Fe_3O_4/AC@ZnO composite.

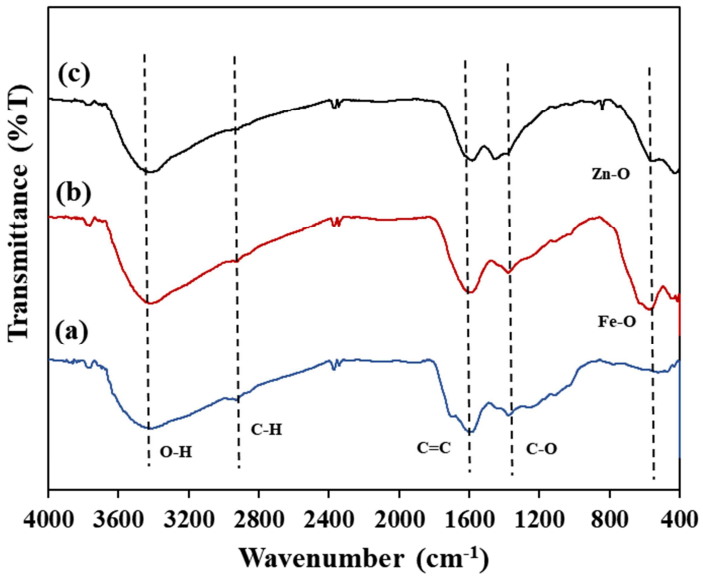

Figure 5: FTIR spectra of (a) activated carbon, (b) Fe_3O_4/AC and (c) Fe_3O_4/AC@ZnO composite.

3.6. Photocatalytic experiment

Figure 6 illustrates the impact of blank, activated carbon, Fe_3O_4/AC, and Fe_3O_4/AC@ZnO on the reduction of dye concentration, both with and without irradiation. The treatment was conducted for 40 min without irradiation first to negate

the adsorption effect, then followed by irradiation with visible light. The reduction (C/Co) for Congo red dye concentration subsequently from the lowest: blank (photolysis) < activated carbon <Fe_3O_4/AC <Fe_3O_4/AC@ZnO composite. The degradation of Congo red dye was nearly nonexistent when subjected to visible light without a catalyst. Photolysis solely depends on light energy to cleave bonds, resulting in more constrained capabilities and a slower reaction rate. The incorporation of ZnO, Fe_3O_4, and activated carbon exhibited synergistic interaction, characterized by robust adsorption and photocatalytic degradation results.

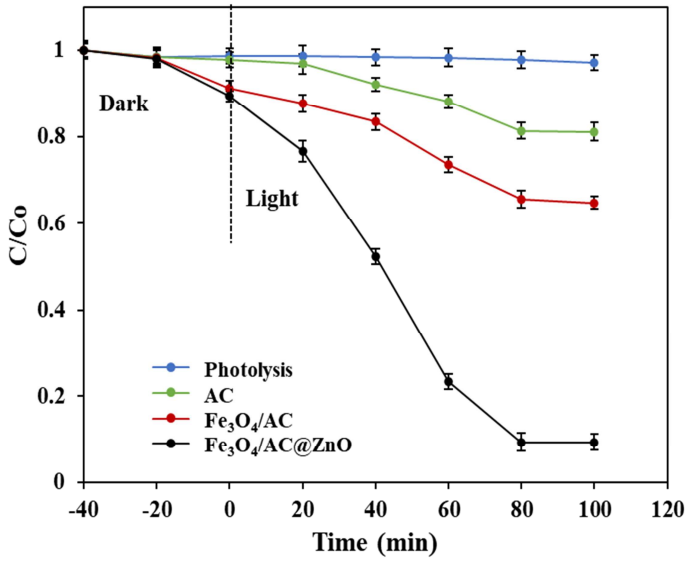

Figure 6: Comparison of Congo red dye degradation, namely blank (photolysis), with the addition of activated carbon, Fe_3O_4/AC, and Fe_3O_4/AC@ZnO composite

The UV-Vis spectrophotometric measurement of Congo red dye is illustrated in Figure 7. The absorption peak of Congo red dye occurs at a wavelength of 498 cm^{-1}. The irradiation duration influences the reduction in absorbance of Congo red dye, resulting from photocatalytic degradation utilizing Fe_3O_4/AC@ZnO under visible light. In photocatalytic degradation, Congo red dye molecules are decomposed into smaller compounds that do not absorb light at the same wavelength. This results in a reduction of dye molecules in the solution, leading to a fall in the absorption value.

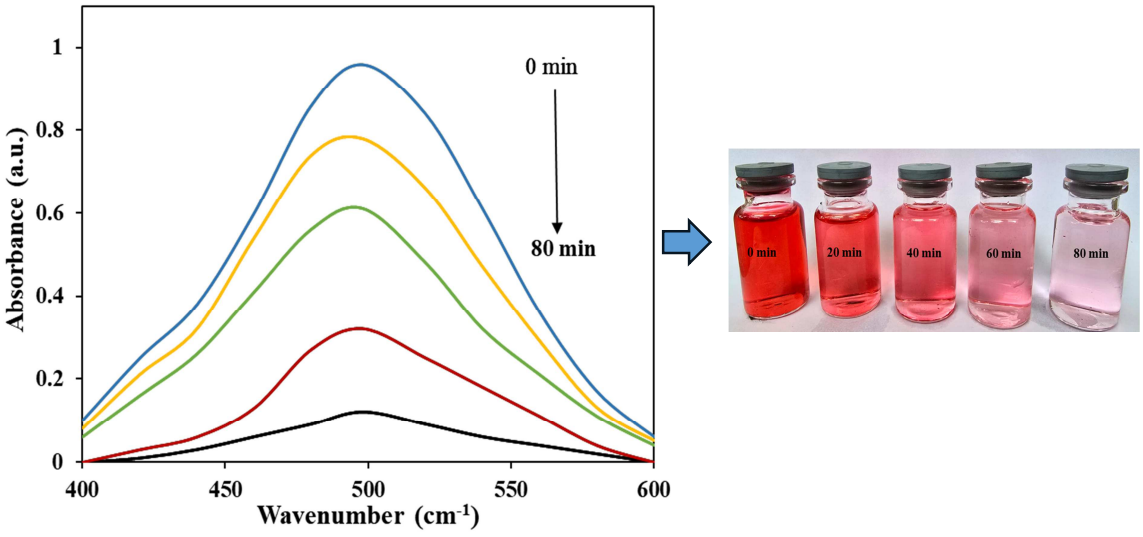

Figure 7: Alterations in the UV-Vis spectrum during the degradation process utilizing Fe_3O_4/AC@ZnOcomposite at a dosage of 0.2 g/L and a concentration of 20 mg/L during varying time intervals.

Figure 8 illustrates the influence of solution pH, composite dosage, dye concentration on degradation efficiency and kinetics model. The pH of the solution is a key parameter that significantly influences the entire photocatalytic process [42,43].The ideal pH for the breakdown of Congo red is between the acidic to neutral range, namely between pH 4 and 7. A number of studies have shown that using ZnONPs/covalent triazine catalysts [44], ZnO [45], and ZIF-67@CeO_2 [46] to break down Congo red dye works best at pH 4.03, 6.63, and 7.0. The Congo red dye possesses an azo structure that can alter its configuration based on the solution's pH. The Congo red dye, with a pKa of 4.0, assumes an anionic form in acidic conditions, forming sulfonate groups that facilitate electrostatic interactions of the dye and the composite surface [22,47]. A pH range from slightly acidic to neutral enhances the generation of hydroxyl radicals (•OH), thereby enhances the breakdown of Congo red dye. At highly acidic pH, ZnO may dissolve to produce Zn^{2+}, hence diminishing its photocatalytic efficacy. With increasing pH, the composite becomes more negative so that repulsion occurs with the dye. Consequently, within the ideal pH range, an equilibrium exists among dye adsorption, hydroxyl radical generation, and the stability of ZnO as a photocatalyst. The optimal pH in this investigation was determined to be 4.

To ascertain the optimal dosage of Fe_3O_4/AC@ZnO composite, degradation was performed with doses ranging from 0.1 g/L to 0.4 g/L at a solution pH of 4 and a dye concentration of 20 mg/L. At low concentrations, insufficient active ZnO sites exist to absorb photons and generate oxidative radicals. At elevated doses, degradation intensifies due to the increase in the number of composites exposed to photons, resulting in the generation of additional radicals such as •OH and O_2• [48]. The optimal dosage achieved was 0.3 g/L. At higher dosages, degradation diminishes since the addition of a catalyst renders the solution turbid, obstructing irradiation to the catalyst surface [49].

The contribution of dye concentration on degradation efficiency was assessed with concentrations varying from 10 to 40 mg/L in the following condition: a solution pH of 4 and a catalyst dosage of 0.3 g/L. The degradation efficiencyis influenced by the initial concentration of the dye; an increase in dye concentration tends to decrease in degradation efficiency[42]. At low concentrations, UV/visible light effectively penetrates the solution, facilitating a higher number of photons reaching the composite, thereby improving degradation efficacy. At high concentrations, the dye solution inhibits light radiation, leading to a reduced number of photons achieving the catalyst surface, which is essential for the radical generation needed for degradation [50]. The degradation efficiencies at concentrations of 20 mg/L, 40 mg/L, 60 mg/L, and 80 mg/L are 99.20%, 90.5%, 81.30%, and 69.40%, respectively.

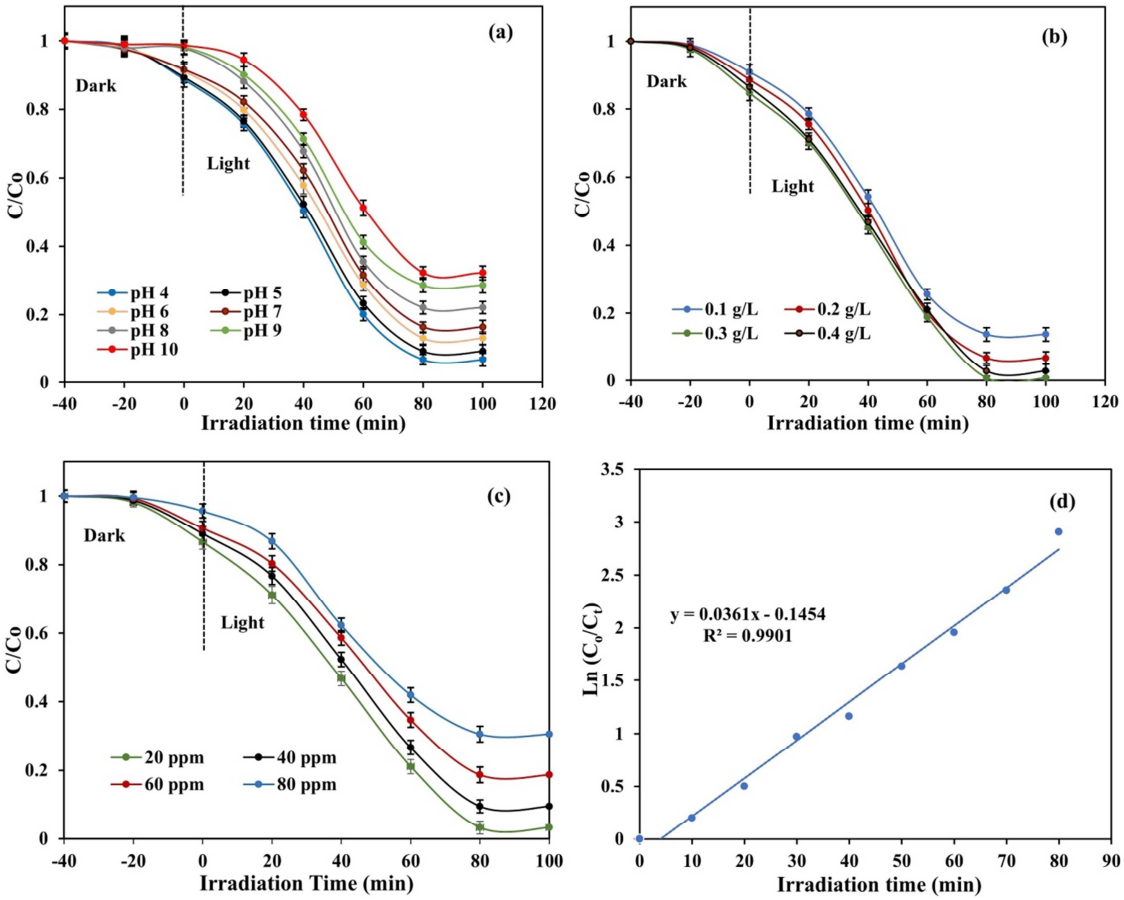

Figure 8: Effect of (a) pH solution, (b) dosage, (c) concentration of dye for C/C_o and (d) the degradation kinetic.

The photocatalytic activity was evaluated by examining the degradation kinetics, utilizing a pseudo-first-order kinetic model expressed by the following equation:

$$ln\frac{C_0}{C} = kt \quad (1)$$

Where C_t and$C$ represent the dye concentration at any given time and the initial dye concentration (mg/L), respectively; k denotes the reaction rate constant (min^{-1}), and t signifies the time (min). This study utilized a dye concentration of 20 mg/L, a solution pH of 4, and a catalyst dosage of 0.3 g/L for the experiment. The coefficient of determination (R^2) was 0.9901, nearing 1, signifying that the pseudo-first-order model aligns well with the experimental data. The k value of 0.0361 min^{-1} exceeds those reported in earlier research, which are 0.0015 min^{-1} for CeO_2 [47] and 0.02455 min^{-1} for 2% Ni-doped γ-Bi_2O_3 [50]. A higher k value signifies a more rapid degradation of the dye, indicating more photocatalytic efficiency.

3.7. Photocatalytic degradation mechanism

The photocatalytic degradation of contaminants organicdepends on the production and reactivity of radicals. A scavenger test was conducted to elucidate the role of Reactive Oxygen Species (ROS) on this mechanism [51]. Figure 9 illustrates that various scavenger agents have distinct degradation efficiencies. The scavenger reagents employed are isopropanol (IPA), benzoquinone (BQ), and ethylenediamine tetraacetic acid (EDTA). The degradation order, in the absence of a scavenger, is as follows: IPA > EDTA > BQ. The reduction in degradation efficiency indicates that the scavengers involved in the degradation process are superoxide anions ($•O_2^-$), followed by hydroxyl radicals (•OH) and holes (h^+). The breakdown of Congo red dye with La–CeO_2 and NiO yielded identical results, indicating that superoxide anions ($•O_2^-$) are the primary agents of degradation [47,52]. Sun et al. [53] propose that the potential degradation mechanism involves superoxide radicals ($•O_2^-$) and hydroxyl radicals (•OH), which initially target the $-NH_2$, $-SO_3^-$ branched chains, and aromatic rings within the Congo red dye molecule. Moreover, the azo link—N=N—is cleaved, resulting in the continual formation of H_2O, CO_2, and minor innocuous molecules [54,55].

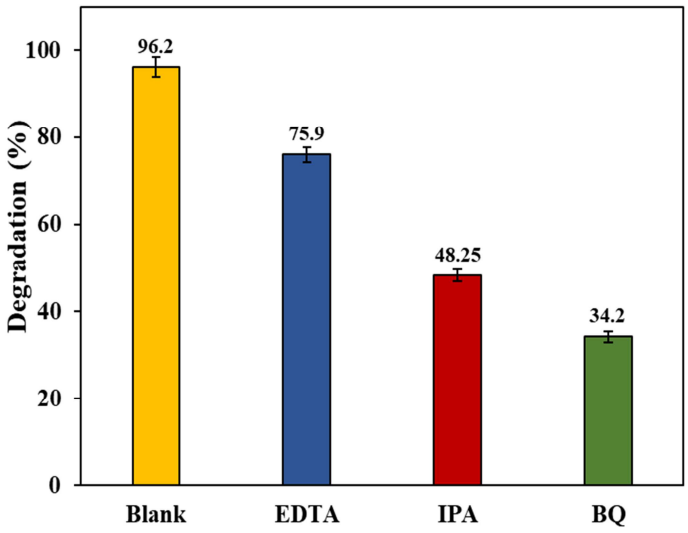

Figure 9: Photocatalytic degradation of Congo red dyewith various radical trapping agents.

The mechanism of Congo red dye degradation by Fe_3O_4/AC@ZnO composite is as follows [52]:

Fe_3O_4/AC@ZnOcomposite $+h\nu \rightarrow e^-_{(CB)} + h^+_{(VB)}$ (2)

$e^-_{(CB)} + h^+_{(VB)} \rightarrow$ energy (3)

$H_2O + h^+_{(VB)} \rightarrow •OH + H^+$ (4)

$O_2 + e^-_{(CB)} \rightarrow •O_2^-$ (5)

Congo red dye + $•OH/•O_2^- \rightarrow H_2O + CO_2$ + other product (6)

3.8. Reusability and stability composite

Evaluating the stability, effectiveness, and recyclability of the catalysts is crucial for practical use and catalyst reuse. The previously utilized catalyst was extracted from the treated dye using centrifugation, subsequently rinsed with ethanol [56]. Then, the composite was dried in an oven at 60°C for 2 h [55]. The degrading efficiency diminished from 97.90% to 92.70% during 5 cycles, reflecting an average decline of 1.04% each cycle (Figure 10). The results demonstrate that the catalyst exhibits excellent stability, hence lowering manufacturing costs since it eliminates the need to purchase a new catalyst for

each reaction. Moreover, it enables implementation on an industrial scale due to the enhanced stability and efficiency of the process. The composite's stability surpassed those of RGO-modified MIL-125(Ti) for the same dye, which diminished from 96.6% to 65.2% during four cycles [57].

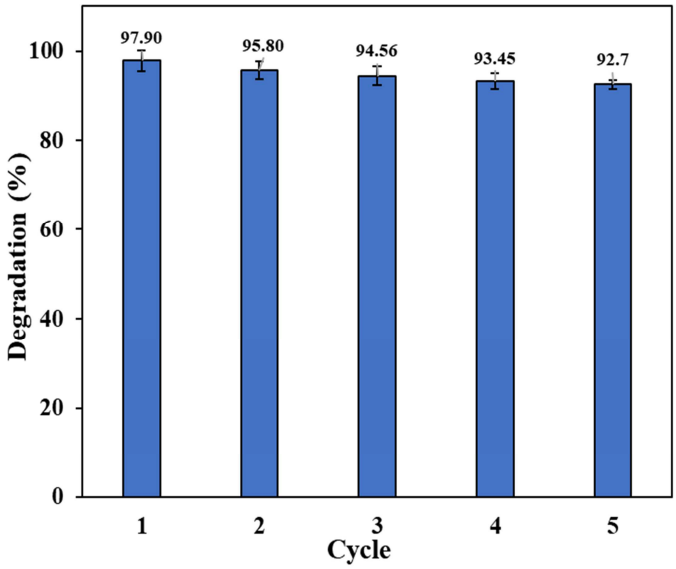

Figure 10: Reusability of Fe_3O_4/AC@ZnOcomposite for photocatalytic degradation of Congo red dye.

4. Conclusion

This study effectively synthesized Fe_3O_4/AC@ZnO composite as a photocatalyst for the degradation of Congo red dye. Activated carbon is produced from bamboo through activation with KOH. Fe_3O_4 and ZnO doping on activated carbon increases the surface area, reduces the band gap, and the composite is magnetic, which facilitates the separation of the composite from the solution after the photocatalytic degradation process. At optimum conditions, namely pH 4, a catalyst dosage of 0.3 g/L, and a dye concentration of 20 mg/L, a degradation efficiency of 99.20% was obtained. The main radical that plays a role in the degradation of Congo red dye is superoxide anion ($\bullet O_2^-$). Fe_3O_4/AC@ZnO composite has outstanding stability, demonstrating a reduction of 5.2% after five cycles of reuse. The findings suggest that the composite has potential for wastewater treatment, especially for those containing organic pollutants.

5. Conflicts of interest

No conflicts exist to declare.

6. Acknowledgment

This research is funded from the DIPA Budget of the Universitas Sriwijaya Public Service Agency for the 2024 Fiscal Year, Unggulan Kompetitif Scheme No. SP DIPA-023.17.2.677515/2024, November 24, 2023. In accordance with the Rector's Decree No. 0013/UN9/LP2M.PT/2024, May 20, 2024.

7. References

[1] Le, T.X.H.; Nguyen, T.V.; Yacouba, Z.A.; Zoungrana, L., Avril, F.; Petit, E.; Mendret, J.; Bonniol, V.; Bechelany, M.; Lacour, S.; Lasage, G.;Cretin, M. Toxicity removal assessments related to degradation pathways of azo dyes: Toward an optimization of Electro-Fenton treatment. *Chemosphere*. 2016, 161, 308–318. https://doi.org/10.1016/j.chemosphere.2016.06.108

[2] Alghanmi, R.M.; Abdelrahman, E. A. Simple production and characterization of ZnO/MgO nanocomposite as a highly effective adsorbent for eliminating Congo red dye from water-based solutions. *Inorg. Chem. Commun*. 2024, 161, 112137. https://doi.org/10.1016/j.inoche.2024.112137

[3] Ozturk, D.; Gulcan, M. Synthesis, characterization, and in-situ H_2O_2 generation activity of activated Carbon/Goethite/Fe_3O_4/ZnO for heterogeneous electro-Fenton degradation of organics from woolen textile wastewater. *J. Ind. Eng. Chem*. 2023, 122, 251–263. https://doi.org/10.1016/j.jiec.2023.02.026

[4] Sayyed, A.J.; Pinjari, D.V.;Sonawane, S.H.; Bhanvase, B.A. Sheikh, J. Sillanpaa, M. Cellulose-based nanomaterials for water and wastewater treatments: A review. *J. Environ. Chem. Eng*.2021, 9(6), 106626. https://doi.org/10.1016/j.jece.2021.106626

[5] Reza, K. M.; Gulshan, F. Parameters affecting the photocatalytic degradation of dyes using TiO_2: a review. *Appl. Water Sci*. 2017, 7, 1569–1578.https://doi.org/10.1007/s13201-015-0367-y
[6] Patel, D.D.; Bhatt, S. Environmental pollution, toxicity profile, and physico-chemical and biotechnological approaches for treatment of textile wastewater. *Biotechnol Genet Eng Rev*. 2022, 38(1), 33–86. https://doi.org/1080/02648725.2022.2048434
[7] Makhtar, S.N.H.H.; Yusof, N.; Fajrina, N.; Hairon, N.H.H.; Aziz, F.; Salleh, W.H.W. V_2O_5/Cds as nanocomposite catalyst for Congo red dye photocatalytic degradation under visible light. *Mater. Today*. 2024, 96, 69–72. https://doi.org/10.1016/j.matpr.2023.10.152
[8] Kaur, S.; Sharma, S.; Kansal, S.K.Synthesis of ZnS/CQDs nanocomposite and its application as a photocatalyst for the degradation of an anionic dye, ARS. *Superlattices Microstruct*. 2026, 98, 86–95. https://doi.org/10.1016/j.spmi.2016.08.011
[9] Lellis, B.; Favaro-Polonia, C.Z.; Pamphile, J.A.; Polonia, J.C. Effects of textile dyes on health and the environment and bioremediation potential of living organisms. *Biotechnol. Res. Innov*. 2019, 3(2), 275–290. https://doi.org/10.1016/j.biori.2019.09.001
[10] Sriram, G.; Uthappa, U.T.; Losic, D.; Kigga, M.; Jung, H.Y.; Kurkuri, M.D. Mg-Allayered double hydroxide (LDH) modified diatoms for highly efficient removal of Congo red from aqueous solution. *Appl. Sci*. 2020, 10(7), 2285. https://doi.org/10.3390/app10072285
[11] Khan, R.R.M.; Qamar, H.; Hameed, A.; Rehman, A.; Pervaiz, M.; Saeed, Z.; Adnan, A.; Rashid Ch, A. Biological and photocatalytic degradation of Congo red, a Diazo sulfonated substituted dye: a review. *Water Air Soil Pollut*. 2022, 233, 468. https://doi.org/10.1007/s11270-022-05935-9
[12] Shetti, N.P.; Malode, S.J.; Malladi, R.S.; Nargund, S.L.; Shukla, S.S.; Aminabhavi, T.M. Electrochemical detection and degradation of textile dye Congo red at graphene oxide modified electrode. *Microchem. J*. 2019, 146, 387–392. https://doi.org/10.1016/j.microc.2019.01.033
[13] Yakupova, E.I.; Bobyleva, L.G.; Vikhlyyantsev, I.M.; Bobylev, A.G.Congo red and amyloids: history and relationship. *Biosci. Rep*.2019, 39(1), BSR20181415. https://doi.org/10.1042/BSR20181415
[14] Igbal, A.; Cevik, E.; Bozkurt, A.; Asiri, S.M.M.; Alagha, O.; Qahtan, T.F.; Jalees, M.I.; Faroog, M.U. Ultrahigh adsorption by regenerable iron-cobalt core-shell nanospheres and their synergetic effect on nanohybrid membranes for removal of malachite green dye. *J. Environ. Chem. Eng*. 2022, 10(3), 107968. https://doi.org/10.1016/j.jece.2022.107968
[15] Bai, H.; Feng, Y.; Zhu, C.; Guo, P.;Wang, J.; Zhou, Y.;Zhang, L.; Li, S.; Chen, J. Efficient adsorption of Congo red (CR) dye onto novel lignin-based magnetic core-shell adsorbent: Synthesis, characterization and experimental studies. *J. Taiwan Inst. Chem. Eng*. 2024, 164, 105689.https://doi.org/10.1016/j.jtice.2024.105689
[16] Jasim, R.A.; Salman, R.H. Congo red removal from aqueous solution by electrocoagulationelectro-oxidation combined system with Al and Cu–Mn–Ni nano composite as efficient electrodes. *Case Stud. Chem. Environ. Eng*. 2024, 9, 100747. https://doi.org/10.1016/j.cscee.2024.100747
[17] Prabhakar, N.; Isloor, A.M.; Padaki, M.; Ismail, A.F. Fabrication of TiO_2@ZIF-67 metal organic framework composite incorporated PVDF membranes for the removal of hazardous reactive black 5 and Congo red dyes from contaminated water. *Chem. Eng. J*. 2024, 498, 155270. https://doi.org/10.1016/j.cej.2024.155270
[18] Das, S.; Bhat, A.P.; Gogate, P.R. Degradation of dyes using hydrodynamic cavitation: Process overview and cost estimation. *J. Water Process Eng*. 2021, 42, 102126. https://doi.org/10.1016/j.jwpe.2021.102126
[19] Rajoriya, S.; Bargole, S.; George, S.; Saharan, V.K. Treatment of textile dyeing industry effluent using hydrodynamic cavitation in combination with advanced oxidation reagents. *J. Hazard. Mater*. 2018, 344,1109–1115. https://doi.org/10.1016/j.jhazmat.2017.12.005
[20] Dehghani, A.; Baradaran, S.; Movahedirad, S. Synergistic degradation of Congo red by hybrid advanced oxidation via ultraviolet light, persulfate, and hydrodynamic cavitation. *Ecotoxicol. Environ. Saf*. 2024, 272, 116042. https://doi.org/10.1016/j.ecoenv.2024.116042
[21] Chen, F.; Yang, Q.; Niu, C.; Li, X.; Zhang, C.; Zhao, J.; Xu, Q.; Zhong, Y.; Deng, Y.; Zeng, G. Enhanced visible light photocatalytic activity and mechanism of $ZnSn(OH)_6$ nanocubes modified with AgI nanoparticles. *Catal. Commun*. 2016, 73, 1–6. https://doi.org/10.1016/j.catcom.2015.10.003
[22] Hariani, P.L.; Salni, Said, M.; Farahdiba, R. Core-shell Fe_3O_4/SiO_2/TiO_2magnetic modified Ag for the photocatalytic degradation of Congo red dye andantibacterial activity.*Bull. Chem. React. Eng*. 2023, 18(2), 315–330. https://doi.org/10.9767/bcrec.19275
[23] Goktas, S.; Goktas, A. Comparative study on recent progress in efficient ZnO based nanocomposite and heterojunction photocatalysts: A review. *J. Alloys Compd*. 2021, 863, 158734. https://doi.org/10.1016/j.jallcom.2021.158734
[24] Liu, Y.; Sun, L.; Wu, J.; Fang, T.; Cai, R.; Ewi, A. Preparation and photocatalytic activity of ZnO/Fe_2O_3 nanotube composites. *Mater. Sci. Eng. B*. 2015, 194, 9–13. https://doi.org/10.1016/j.mseb.2014.12.021
[25] Zhu, P.; Hu, M.; Duan, M.; Xie, L.; Zhao, M. High visible light response Z-scheme Ag_3PO_4/g-C_3N_4/ZnO composite photocatalyst for efficient degradation of tetracycline hydrochloride: Preparation, properties and mechanism. *J. Alloys Compd.* 2020, 840, 155714. https://doi.org/10.1016/j.jallcom.2020.155714
[26] Zhang, H.; Jia, Z. Application of porous silicon microcavity to enhance photoluminescence of ZnO/PS nanocomposites in UV light emission. *Optik*. 2017, 130, 1183–1190. https://doi.org/10.1016/j.ijleo.2016.11.131
[27] Liu, J.; Xia, Q.; Chen, C. Graphene oxide enhanced the photocatalytic performance of one-dimensional porous carbon/ZnO hybrids. *Vacuum*. 2024, 228, 113528. https://doi.org/10.1016/j.vacuum.2024.113528

[28] Yang, K.;Deng, R.; Wang, C.; Wu, S.; Cui, Z.; Zheng, Y.; Li, Z.; Jiang, H.; Zhu, S.;Chu, P.K.; Liu, X. CuO/ZnO heterojunction nanofilm for effective photocatalytic disinfection. *Surf. Interfac*. 2024, 53, 105023. https://doi.org/10.1016/j.surfin.2024.105023

[29] Alkalin, S.A.;Yavas, A.; Guler, S.; Erol, M.Photocatalytic activities of Fe_2O_3 coated ZnO nanowires grown by electrochemical anodization method. *Ceram. Int*. 2024, 50, 39278–39284. https://doi.org/10.1016/j.ceramint.2024.07.298

[30] Aliah, H.; Rini, N.P.;Farouk, I.S.;Zurnansyah, Mahardhika, L.J.; Jayanti, P.D.;Kusumah, H.P.;Tumbelaka, R.M.;Istiqomah, N.I.;Asri, N.S.; Iman, R.N.;Suharyadi, E. Microstructures, optical, magnetic properties, and photocatalytic activity of magnetically separable and reusable ZnO-Doped Fe_3O_4/rGO nanocomposite synthesized via green rout. *Carbon Resour. Convers.*2024, 7, 100235. https://doi.org/10.1016/j.crcon.2024.100235

[31] Ozchan, M. Photocatalytic activity of green synthesis ZnO nanoparticles from chitosanand investigating the growth mechanism. *J. Mol. Struct.* 2025, 1321, 140020. https://doi.org/10.1016/j.molstruc.2024.140020

[32] Kaewtrakulchai, N.;Chanpee, S.;Jadsadajerm, S.;Wongrerkdee, S.;Manatura, K.;EiadUa, A., Co-hydrothermal carbonization of polystyrene waste and maize stover combined with KOH activation to develop nanoporous carbon as catalyst support for catalytic hydrotreating of palm oil. *Carbon Resour. Convers*. 2024, 7, 100231. https://doi.org/10.1016/j.crcon.2024.100231

[33] Chanpee, S.;Kaewtrakulchai, N.;Khemasiri, N.; Eiad-Ua, A.;Assawasaengrat, P. Nanoporous carbon from oil palm leaves via hydrothermal carbonization-combined KOH activation for paraquat removal. *Molecules*. 2022, 27, 5309. https://doi.org/10.3390/molecules27165309.

[34] Machrouchi, A.;Khiar, H.;Elhalil, A.; Sadiq, M.;Abdennouri, M.; Barka, N. Synthesis, characterization, and photocatalytic degradation of anionic dyes using a novel ZnO/activated carbon composite. *Watershed Ecol. Environ*. 2023, 5, 80–87. https://doi.org/10.1016/j.wsee.2022.12.001

[35] Jayarambabu, N.; Rao, N.V.S.S.S.;Sivalenka, M.K.C.; Saraswathi, K.;Naick, B. S.; Anitha, N.; Rao, T.V. Bamboo-derived activated carbon-functionalized ZnO NPs for non-enzymatic glucose sensing. *Diam. Relat. Mater.* 2024, 144, 110959. https://doi.org/10.1016/j.diamond.2024.110959

[36] Zaoui, F.;Sebba, F.Z.; Liras, M.; Sebti, H.;Hachemaoui, M.; Mokhtar, A.; Beldjilali, M.;Bounaceur, B.;Boukoussa, B. Ultrasonic preparation of a new composite poly(GMA)@Ru/TiO_2@Fe_3O_4: Application in the catalytic reduction of organic pollutants. *Mater. Chem. Phys*.2021, 260, 124146. https://doi.org/10.1016/j.matchemphys.2020.124146

[37] Foroutan, R.; Mohammadi, R.; Ahmadi, A.;Bikhabar, G.; Babaei, F.;Ramavandi, B. Impact of ZnO and Fe_3O_4 magnetic nanoscale on the methyl violet 2B removal efficiency of the activated carbon oak wood. *Chemosphere*. 2022, 286, 131632. https://doi.org/10.1016/j.chemosphere.2021.131632

[38] Ma, M.; Ying, H.;Cao, F.; Wang, Q.; Ai, N. Adsorption of Congo red on mesoporous activated carbon prepared by CO_2 physical activation. *Chin. J. Chem. Eng*.2020, 28(4), 1069–1076.https://doi.org/10.1016/j.cjche.2020.01.016

[39] Tumbelaka, R.M.;Istiqomah, N.I.; Kato, T.;Oshima, D.;Suharyadi, E. High reusability of green-synthesized Fe_3O_4/TiO_2 photocatalyst nanoparticles for efficient degradation of methylene blue dye. *Mater. Today Commun*. 2022, 33, 104450. https://doi.org/10.1016/j.mtcomm.2022.104450

[40] Alghanmi, R.M.; Abdelrahman, E.A. Simple production and characterization of ZnO/MgO nanocomposite as a highly effective adsorbent for eliminating Congo red dye from water-based solutions. *Inorg. Chem. Commun*. 2024, 161, 112137. https://doi.org/10.1016/j.inoche.2024.112137

[41] Harimisa, G.E.; Jusof, N.W.C.; Tan, L.S.; Ghafar, N.A. Influence of furnace atmospheres and potassium hydroxide activation on the properties of bamboo activated carbon and its adsorption towards 4-nitrophenol. *Chem. Eng. Res. Des.* 2023, 198, 325–339.https://doi.org/10.1016/j.cherd.2023.09.008

[42] Enas, A.; Marwa, S.S. Facile green synthesis of ZnOsupported on exfoliated graphite for photocatalytic degradation of dye under UV and Visible-light irradiation. *Egypt. J. Chem*. 2022, 65, 557–569. https://doi.org/10.21608/EJCHEM.2022.130532.5931

[43] Ibtisam, A.; Souad, A.E.; Amr, A.E.; Gamal, E. Cetyltrimethylammonium bromide@$CoFe_2O_4$nanocomposite for photocatalyticreduction of Cr(VI) employing a simple colorimetry assay. *Egypt. J. Chem*. 2025, 68, 295–303. https://doi.org/10.21608/ejchem.2024.279458.9530

[44] Moeinzadeh, R.; Azizi, N.; Hekmati, M.;Qomi, M.;Esmaeili, D. ZnONPs/covalent triazine frameworks nanocomposite as high-performance photocatalysts for degradation of Congo red under visible light. *Mater. Chem. Phys*. 2023, 307, 128122. https://doi.org/10.1016/j.matchemphys.2023.128122

[45] Yashni, G.; Al-Gheethi, A.; Mohamed, R.M.S.R.;Dai-Viet, N.V.;Al-Kahtami, A.A.; Al-Sahari, M.;Hazhar, N.J.N.; Noman, E.;Alkhadher, S.Bio-inspired ZnO NPs synthesized from Citrus sinensis peels extract for Congo red removal from textile wastewater via photocatalysis: Optimization, mechanisms, techno-economic analysis. *Chemosphere*. 2021. 281, 130661. https://doi.org/10.1016/j.chemosphere.2021.130661

[46] Tong, L.; Li, Z.; Ma, Y.; Zhao, L. Synthesis of CeO_2-loaded composite catalysts of ZIF-67 for activation of persulfate degradation of Congo red dye. *Colloids Surf. A: Physicochem. Eng*. 2024, 685, 133189. https://doi.org/10.1016/j.colsurfa.2024.133189

[47] Rianjanu, A.;Marpaung, K.D.P.;Siburian, C.; Muhtar, S.A.;Khamidy, N.I.;Widakdo, J.; Yulianto, N.; Aflaha, R.;Triyana, K.; Taher, T. Enhancement of photocatalytic activity of CeO_2 nanorods through lanthanum doping (La–CeO_2) for the degradation of Congo red dyes. *Results Eng*. 2024, 23, 102748. https://doi.org/10.1016/j.rineng.2024.102748

[48] Boudiaf, S.; Nasrallah, N.; Mellal, M.;Behamdi, B.; Belabed, C.;Djilali, M.A.; Trari, M. Kinetic studies of Congo red photodegradation on the hetero-system $CoAl_2O_4$/ZnO with a stirred reactor under solar light. *J. Environ. Chem. Eng*. 2021, 9, 105572. https://doi.org/10.1016/j.jece.2021.105572

[49] Khan, S.; Khan, A.; Ali, N.;Ahmad, S.; Ahmad, W.; Malik, S.; Ali, N.; Khan, H.; Shah, S.; Bilal, M. Degradation of Congo red dye using ternary metal selenide-chitosan microspheres as robust and reusable catalysts. *Environ. Technol. Innov*. 2021, 22, 101402. https://doi.org/10.1016/j.eti.2021.101402

[50] Jaison, A.; Lee, H.U.; Hur, J.; Mohan, A.;Lee, Y. Facile synthesis of Ni-doped tetrahedral γ-Bi_2O_3 and selective photocatalytic degradation of Congo red under simulated sunlight. *J. Alloys Compd*, 2024, 1004, 175727. https://doi.org/10.1016/j.jallcom.2024.175727

[51] Ahmed, M.A.; Ahmed, M.A.; Mohamed, A.A. Fabrication of NiO/g-C_3N_4 Z-scheme heterojunction for enhancedphotocatalytic degradation of methylene blue dye. *Opt. Mater*. 2024, 151, 115339. https://doi.org/10.1016/j.optmat.2024.115339

[52] Madasamy, S.;Ramananthatheerthan, A.;Marikani, K.;Venugopal, D.;Aldhayan, S.H.A.; Al-Dayan, N.;Palanivelu, S.;Dhanasekaran, S. Biofabrication of nickel oxide nanoparticles from *Pedalium Murex* leaf extract: A promising approach for biomedical andenvironmental applications. *Surf. Interfac*. 2023, 40, 103087. https://doi.org/10.1016/j.surfin.2023.103087

[53] Sun, F.; Qiu, F.; Pan, Y.; Shi, H.; Wang, Y.; Liang, Q.; Hu, S.; Guo, Q.; Dai, M.; Xue, Z. Tubular Ni-NiO-TiO_2 for rapid degradation of Congo red in water under visible light. *Vacuum*, 2025, 233, 113940. https://doi.org/10.1016/j.vacuum.2024.113940

[54] Indira, K.; Shanmugam, S.; Hari, A.;Vasantharaj, S.;Sathiyavimal, S.;Brindhadevi, K.; Askary, A.E.;Elfasakhany, A.; Pugazhendhi, A. Photocatalytic degradation of Congo red dye using nickel–titanium dioxide nanoflakes synthesized by *Mukiamadrasapatna* leaf extract.*Environ. Res*. 2021, 202, 111647. https://doi.org/10.1016/j.envres.2021.111647

[55] Gadore, V.; Singh, A.K.;Mishra, S.R.;Ahmaruzzaman, Md.RSM approach for process optimization of the photodegradation of Congo red by a novel $NiCo_2S_4$/chitosan photocatalyst. *Sci. Rep*, 2024, 14, 1118. https://doi.org/10.1038/s41598-024-51618-2

[56] Abdelbar, N.M.; Ahmed, M.A.; Mohamed, A.A. A novel layered double hydroxide-based ternary nanocomposite for the effective photocatalytic degradation of rhodamine B. *RSC Adv*. 2024, 14, 15523. https://doi.org/10.1039/d4ra00685b

[57] Fatima, R.; Afridi, M.N.;Mohdeb, I.; Madhusudan, P.;Hwang, Y. Photocatalytic degradation of Congo red using RGO-modified MIL-125(Ti) under visible light. *J. Water Process Eng*. 2025,69, 106893. https://doi.org/10.1016/j.jwpe.2024.106893